

Article

Orthorhombic $\text{YBa}_2\text{Cu}_3\text{O}_{7-\delta}$ Superconductor with TiO_2 Nanoparticle Addition: Crystal Structure, Electric Resistivity, and AC Susceptibility

Fatma Barood¹, Mohd Mustafa Awang Kechik^{1,*} , Tan Sin Tee¹, Chen Soo Kien¹ , Lim Kean Pah¹ , Kai Jeat Hong¹, Abdul Halim Shaari¹, Hussein Baqiah², Muhammad Khalis Abdul Karim¹ , Muhammad Kashfi Shabdin¹, Khairul Khaizi Mohd Shariff³, Azhan Hashim⁴ , Nurbaisyatul Ermiza Suhaimi⁴ and Muralidhar Miryala⁵ 

- ¹ Laboratory of Superconductor & Thin Films, Department of Physics, Faculty of Science, Universiti Putra Malaysia, Serdang 43400, Selangor, Malaysia; fatmali2882005@gmail.com (F.B.); tansintee@upm.edu.my (T.S.T.); chensk@upm.edu.my (C.S.K.); limkp@upm.edu.my (L.K.P.); kaijeataaron94@gmail.com (K.J.H.); ahalim@upm.edu.my (A.H.S.); mkhalis@upm.edu.my (M.K.A.K.); kashfi.shabdin@upm.edu.my (M.K.S.)
- ² Shandong Key Laboratory of Biophysics, Institute of Biophysics, Dezhou University, No. 566 University Rd. West, Dezhou 253023, China; husseinbaqiah@gmail.com
- ³ Microwave Research Institute, Universiti Teknologi MARA, Shah Alam 40450, Selangor, Malaysia; khairulkhaizi@uitm.edu.my
- ⁴ Faculty of Applied Sciences, Universiti Teknologi MARA Pahang, Bandar Pusat Jengka 26400, Pahang, Malaysia; dazhan@uitm.edu.my (A.H.); ersyamiza@gmail.com (N.E.S.)
- ⁵ Materials for Energy and Environmental Laboratory, Superconducting Materials, Shibaura Institute of Technology, 3 Chome-7-5 Toyosu, Koto, Tokyo 135-8548, Japan; miryala1@shibaura-it.ac.jp
- * Correspondence: mmak@upm.edu.my



Citation: Barood, F.; Kechik, M.M.A.; Tee, T.S.; Kien, C.S.; Pah, L.K.; Hong, K.J.; Shaari, A.H.; Baqiah, H.; Karim, M.K.A.; Shabdin, M.K.; et al. Orthorhombic $\text{YBa}_2\text{Cu}_3\text{O}_{7-\delta}$ Superconductor with TiO_2 Nanoparticle Addition: Crystal Structure, Electric Resistivity, and AC Susceptibility. *Coatings* **2023**, *13*, 1093. <https://doi.org/10.3390/coatings13061093>

Academic Editor: Alexandru Enesca

Received: 3 May 2023

Revised: 6 June 2023

Accepted: 9 June 2023

Published: 13 June 2023



Copyright: © 2023 by the authors. Licensee MDPI, Basel, Switzerland. This article is an open access article distributed under the terms and conditions of the Creative Commons Attribution (CC BY) license (<https://creativecommons.org/licenses/by/4.0/>).

Abstract: This article reports the effect of a nanoscale addition of TiO_2 on the structure and superconducting parameters of the high-temperature superconductor $\text{YBa}_2\text{Cu}_3\text{O}_{7-\delta}$ (Y123). Polycrystalline compounds of Y123 with different percentages of TiO_2 , $x = 0.0, 0.2, 0.4, 0.6, 0.8,$ and 1.0 , were fabricated using the thermal treatment method. An analysis using X-ray diffraction confirmed the formation of Y123 phases for all composite samples. Field-emission scanning electron microscopy (FESEM) analysis revealed the growth of grain size and decrease in porosity, with a sign of partial melting of grains for the samples with TiO_2 addition. The magnetic and electric transport properties were investigated using AC susceptibility measurement and the four-probe method, respectively. It was observed that the superconducting transition temperature, $T_{c\text{-onset}}$, for a pure sample determined by ACS and 4PP was 95.6 K and 95.4 K, respectively. These values were found to decrease with the addition of TiO_2 , while the superconducting transition (ΔT_c) improved with TiO_2 addition except for the sample at $x = 0.2$ wt.%, which showed the broadest transition width. The sharpest superconducting transition (ΔT_c) was observed for the sample at $x = 1.0$ wt.%, indicating that the addition of TiO_2 nanoparticles is expected to serve as artificial pinning centres and strengthen the connection among the grains in the Y123 ceramic.

Keywords: $\text{YBa}_2\text{Cu}_3\text{O}_{7-\delta}$ superconductor; TiO_2 addition; critical temperature; AC susceptibility

1. Introduction

Since Chu [1] discovered the $\text{YBa}_2\text{Cu}_3\text{O}_{7-\delta}$ (YBCO) superconductor in 1987, there has been considerable interest in the physics and applications of this system, leading to many research efforts. This compound is a type-II superconductor and exhibits a critical temperature transition, T_c , that can reach 92 K, which is higher than liquid nitrogen's temperature ($T_c = 77$ K), making it attractive for the demands of practical applications [2,3]. The requirements of the Y123 applications would not be achieved just by a high T_c ; a

larger critical current density, J_c , in the presence of a magnetic field is crucial for the Y123 compound's optimum performance. However, poor vortex pinning and weak grain couplings contribute to low J_c , hence limiting the use of Y123 material [4,5]. By introducing effective flux-line pinning, it is possible to prevent vortex motion and enhance the critical current density. In addition, it will be essential to fabricate samples with artificial pinning sites in order to improve the critical current density.

It has been widely reported that the incorporation of nano-sized precursors into YBCO bulk could be a significant way to enhance J_c with strong pinning, mainly at high magnetic fields. The flux pinning enhancement can be optimised when the inclusion of nano-sized particles is in the range of the superconducting coherence length of YBCO (2–4 nm) [6]. A significant growth in terms of improvement of the interconnectivity and the flux pinning has been reported by adding various impurities to YBCO, e.g., Y_2O_3 , DY_2O_3 , CO, WO_3 , and Al_2O_3 [7–11]. These metal oxides can act as artificial pinning centres for high critical current density. Among various nanostructure materials, titanium oxide nanoparticles (TiO_2) have attracted the interest of several researchers studying superconductivity. Recently, TiO_2 has demonstrated its potential as a highly effective candidate for reinforcing superconductor ceramics. Therefore, several studies were conducted using TiO_2 as an additive to some of the superconducting compounds, such as MgB_2 [12–14], BPSCCO [15], Bi-2212, and Bi-2223 [16]. The effect of TiO_2 addition on the YBCO bulk has been reported a few times using a variety of synthesis methods. It has been found that the characteristics of the YBCO material are significantly influenced by the synthesis method and the amount of TiO_2 nanoparticles. Based on the various addition levels, significant results have been achieved by many research groups with regards to both critical temperature and critical current. Ghahramani et al. [17] studied the effect of TiO_2 on the superconducting parameters of Y123 prepared via the solid-state method. The T_c increased from 95.50 K for a pure sample to 97.77 K at $x = 0.30$ wt.% of TiO_2 , whereas J_c decreased with the TiO_2 addition compared to the pure sample. Rejith et al. [18] reported the improvement in J_c of Y123 by TiO_2 inclusion, while T_c was slightly decreased from 92 to 90.5 K. It was also found that the flux pinning force was eight times stronger than that in the pure YBCO sample. Hannachi et al. [19] investigated the impact of TiO_2 nanoparticle addition on the intra-granular and inter-granular properties of Y123. The addition of TiO_2 served as efficient pinning centres in the YBCO system, which consequently improved the connectivity between the grains of YBCO. The calculated critical current density, $J(0)_{c, inter}$, was enhanced and was higher by three at $x = 0.1$ wt.% of the TiO_2 addition sample compared to the non-added one. Kebbede et al. [20] studied the anisotropic grain growth of Y123 with (2.5 and 5 mol%) TiO_2 nanoparticles incorporated via the sol-gel coating method. The critical onset temperature, $T_{c-onset}$, was decreased for the 2.5 mol% TiO_2 -coated sample, whereas the normal-state resistivity was higher with a 5 mol% addition due to the presence of the Y211 and $BaCuO_2$ secondary phases. Therefore, the anisotropic grain growth of YBCO was enhanced at lower levels of TiO_2 addition. The use of TiO_2 nanoparticles as an additive in YBCO has proven to be an effective way of enhancing its performance. Therefore, more research is required to accurately validate the effect of TiO_2 addition.

Investigations into this material are still being conducted, in particular based on various doping rates and novel technological uses. Generally, the method of preparation and the nature of the addition have a significant impact on the properties of superconducting materials. The main focus of this study is to apply the thermal treatment technique to prepare Y123 doped with TiO_2 nanoparticles. To our knowledge, however, no literature has reported the use of TiO_2 as an addition to YBCO by using thermal treatment as a preparation method. This method was previously found to have the advantages of being simple, inexpensive, and capable of producing fine powders [21–24]. Thus, the objective of the present study is to investigate the influence of various amounts of TiO_2 nanoparticles ($x = 0.0, 0.2, 0.4, 0.6, 0.8,$ and 1.0 wt.%) on the structure and superconductivity of the Y123 superconductor prepared using the thermal treatment method. Investigations were conducted on phase formation, chemical composition, AC susceptibility, and electrical resistivity.

2. Materials and Methods

The samples of Y123 pellets with different values of TiO₂ were synthesised using a thermal treatment method that uses PVP as a capping agent to reduce agglomeration [25]. The starting compositions of high-purity raw materials from Haverhill, MA, Alfa Aesar, Y(NO₃)₂·6H₂O (99.99%), Ba (NO₃)₂ (99.95%), and Cu (NO₃)₂·2.5H₂O (98%) powders with the appropriate stoichiometric atomic ratio of 1:2:3, were dissolved in 300 mL of deionised water and 6 g of PVP (C₆H₉NO)₆. The mixed solution was heated at 80 °C for 2 h with the help of a magnetic stirrer hot plate. The solution was dried in an oven at 110 °C for 24 h to allow for water evaporation. The resultant green gel was ground for around 1 h using a mortar and pestle until a fine powder formed. Then, the powder was pre-calcined at 600 °C for 4 h using a box furnace and reground again for 15 min before a second calcination was conducted in a double-tube furnace of Model CMTS TF 40/360 at 910 °C for 24 h. The obtained powder after second calcination was mixed with the required wt.% of TiO₂ during the grinding process to be pressed into 13 mm diameter pellets and sintered at 980 °C for 24 h. Extra annealing was conducted at 650 °C for 12 h in an oxygen-rich environment, followed by cooling at 1 °C per hour to prevent oxygen deprivation.

The sintered samples were examined using X-ray diffraction (XRD, Xpert Pro Analytical Philips DY 1861 diffractometer, Phillips, Eindhoven, The Netherlands) with a CuK α source from $2\theta = 20^\circ$ to 80° to evaluate phase identification and the crystal structure of the sample. The microstructure analysis was performed using a field-emission scanning electron microscope along with an energy-dispersive X-ray spectrometer for quantitative analyses (FESEM, FEI Nova NanoSEM 230, Thermo Fisher Scientific, Waltham, MA, USA). Measurement of electric transport properties was conducted in the temperature range 30–280 K with the four-point probe technique using a digital nanovoltmeter (Keithley, Model 2182A, Cleveland, OH, USA) and a DC precision power source (Keithley, Model 6221, Cleveland, OH, USA). The measurements involved determine the values of onset critical temperature, $T_{c-onset}$, and offset critical temperature, $T_{c-offset}$. The temperature dependence of AC susceptibility was investigated using a susceptometer from Cryo Industry, model number REF-1808-ACS (ACS, CryoBIND T, CryoBIND, Zagreb, Croatia). The frequency of the AC signal was 295 Hz, and a magnetic field of 5 Oe was applied.

3. Result and Discussion

3.1. XRD Analysis

Figure 1a describes the Rietveld refinement and fitted XRD profile of Y123/(TiO₂) x patterns, where $x = 0.0, 0.2, 0.4, 0.6, 0.8,$ and 1.0 wt.%. The XRD diffraction peaks for all samples exhibited an orthorhombic perovskite structure and belong to space group Pmmm 47 symmetry with ICSD No. 98-002-1157. The (013 and 103) diffraction peaks, which are characteristic of the YBCO phase, can be observed clearly in both non-added and TiO₂-added samples. A small amount of impurity phase (indicated as Y211 in the figure) was observed for all added TiO₂ patterns. However, there were no detected peaks attributed to TiO₂ addition even with a high percentage of TiO₂ nanoparticles which accords with previous outcomes stated by [18,26]. The absence of TiO₂ nanoparticle structure in the XRD pattern can be attributed to the mixing effect behaviour, which is due to the relatively higher concentration of the Y123 phase compared to the TiO₂. The strong diffraction peaks from the Y123 components can overshadow or mask the weaker diffraction peaks from TiO₂ nanoparticles, making it challenging to observe the TiO₂ crystal structure in the XRD pattern. Our results showed that the diffraction peaks increased in intensity for all TiO₂-added samples, particularly at $x = 0.4$ wt.% TiO₂ concentration, with a noticeable shift of the peak position to the high angle, as presented in Figure 1b. This might be related to thermal cycle stress or the powder pelletising process [27].

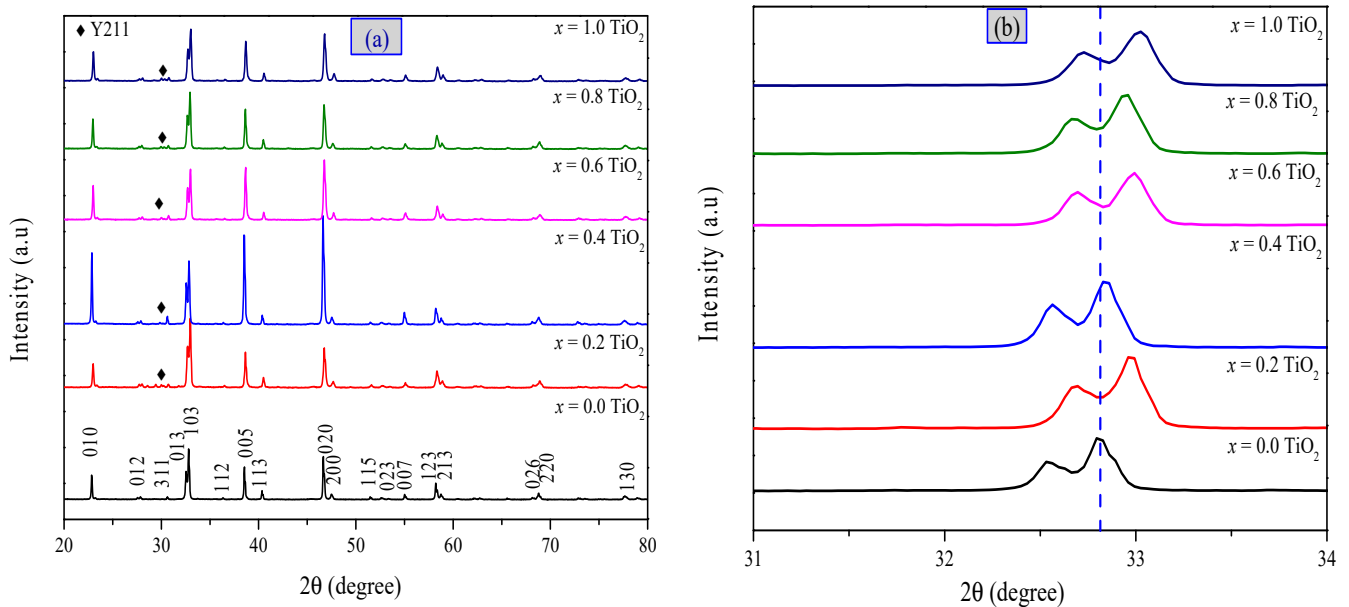


Figure 1. (a) XRD patterns of Y123 samples with different wt.% of TiO₂ nanoparticles; (b) XRD patterns of the peaks related to the (013) and (103) planes of Y123 with wt.% TiO₂ nanoparticles.

The variation of the lattice parameters a , b , and c with TiO₂ concentration is shown in Table 1. It is noticed that the lattice parameter a basically remained the same, while the values of the lattice parameters b and c increased with TiO₂ addition level. These differences in the lattice constants a and b resulted in increased orthorhombicity $(a - b)/(a + b)$ of the superconducting phase. The crystallite size of all added samples was reduced as a result of adding TiO₂, which limited the crystallite growth of the Y123 ceramic. The oxygen stoichiometry, which is known to play a crucial role in the superconducting properties of YBCO [28], was calculated for all sintered samples. The oxygen content of Y123 samples was estimated from the c -axis value using the relation $7 - \delta = 75.25 - 5.856c$ [29]. It was noticed that the oxygen content decreased for all Y123/TiO₂ composites. The relation between parameter c -axis and oxygen level is also consistent with the typical behaviour of c -axis in the orthorhombic phase Y123, as it is well known that the c -axis parameter increases when the oxygen content decreases [29]. The crystallite size, orthorhombicity, and oxygen content values are tabulated in Table 1.

Table 1. Lattice parameters a , b , and c , orthorhombicity, crystallite size, and oxygen content of Y123 with various wt.% of TiO₂.

TiO ₂ ($x = \text{wt.}\%$)	a (Å)	b (Å)	c (Å)	Orthorhombicity (10^{-3})	Crystallite Size (nm)	Oxygen Content
0.0	3.827	3.885	11.672	7.520	180	6.89
0.2	3.828	3.889	11.695	7.904	72.7	6.76
0.4	3.826	3.889	11.683	8.163	91.0	6.83
0.6	3.824	3.888	11.690	8.298	81.2	6.79
0.8	3.829	3.890	11.691	7.902	78.1	6.78
1.0	3.825	3.889	11.695	8.295	70.2	6.76

3.2. Microstructure Analysis

The FESEM analysis was conducted to further investigate the impact of TiO₂ nanoparticle addition on the microstructure of YBCO samples. Figure 2a–f shows the surface morphology of the Y123/(TiO₂) x composite along with EDX spectra and histograms of the average grain size distribution. As can be seen, the surface morphology was modified under TiO₂ inclusion compared to pure one. The grain boundaries were defined as

a granular microstructure with shaped rectangular grains distributed uniformly among the sample. The grains were closely packed and elongated with the addition of TiO_2 . In addition, a sign of partial melting was observed in the grains, leading to the presence of a poorly defined grain boundary. This indicated the fusion of several neighbouring grains, leading to an increase in grain size during melting [30]. The average grain size was 1.59, 2.82, 2.50, 2.74, 3.04, and 2.48 μm for the samples with $x = 0.0, 0.2, 0.4, 0.6, 0.8,$ and 1.0 , respectively. It is clearly evident that the addition of TiO_2 increased the grain size of different sintered Y123 samples. It is thought that in ceramic materials, higher sintering temperatures cause partial melting and merging of the grain boundaries, which promote grain size growth [31,32]. As a result, no pores were detected in these composite samples because the grains of Y123 continued to grow and filled the gaps among the grains. On the other hand, the increase in grain size with TiO_2 can create better inter-grain connections, allowing the flow of inter-grain electric current. Hence, the transport critical current J_c is expected to increase with TiO_2 additive.

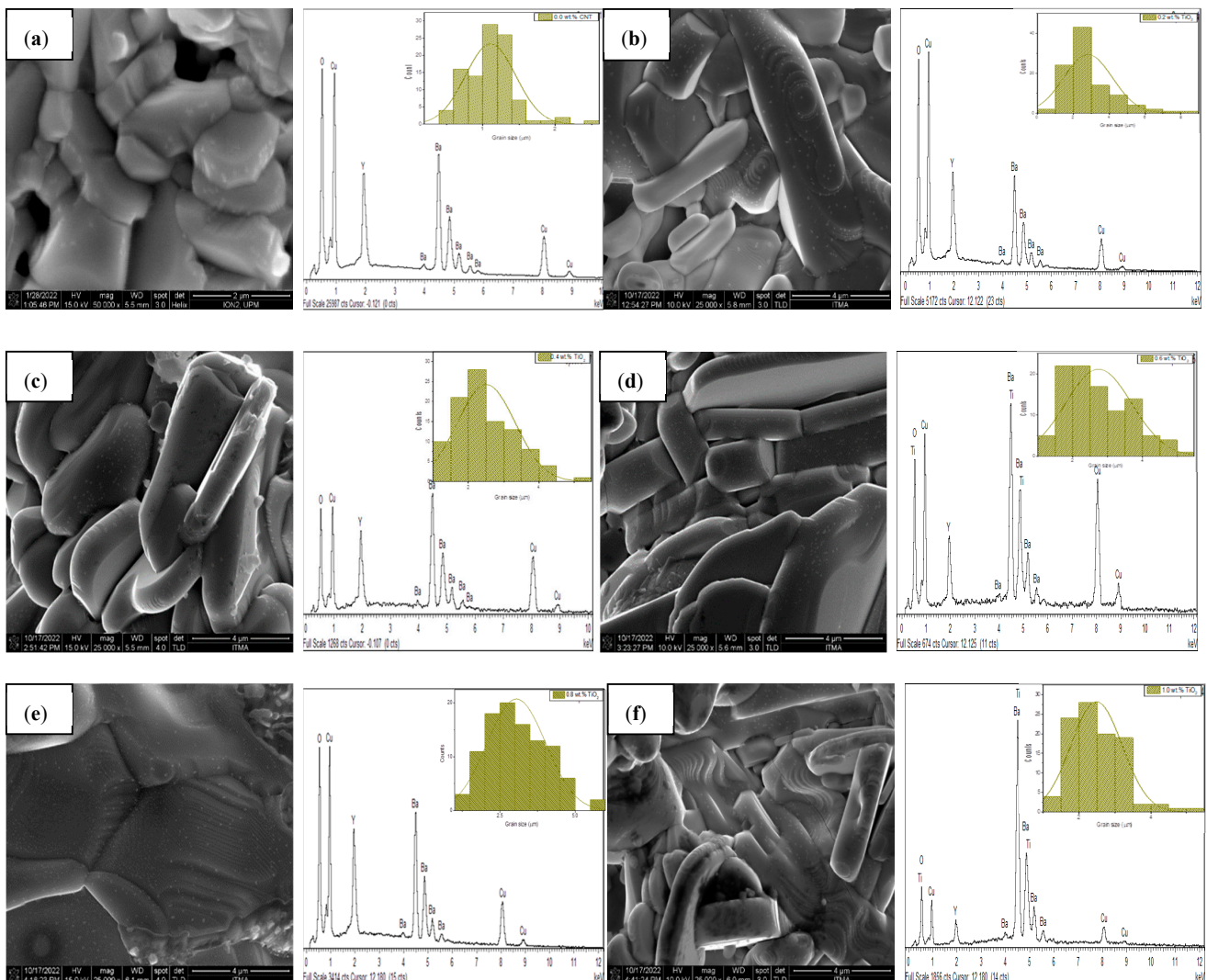


Figure 2. (a–f): FESEM images of surface morphology and EDX spectra along with histograms of average grain size distribution of Y123 with $x = 0.0, 0.2, 0.4, 0.6, 0.8,$ and 1.0 wt.% of TiO_2 addition.

Figure 2a–f displays EDX spectra along with a histogram of the average grain size distribution for each sample of Y123/ TiO_2 composites at $x = 0.0, 0.2, 0.4, 0.6, 0.8,$ and 1.0 wt.%. The EDX analysis confirmed the presence of the elements Y, Ba, Cu, and O for all the samples, as reported in Table 2. The atomic ratios for Y:Ba: Cu were matched to

the main composition of 1:2:3. The spectra graph of EDX also detected Ti ion peaks for 0.6 and 1.0 wt.%, while it was not detected in the other percentages. The limited resolution in space of the analysis and the limited sample area selected for EDX analysis may result in variations in the detected elemental composition, as the analysed regions are only point-sized. Consequently, there is a possibility of missing Ti particles or areas that contain Ti but may be present in other regions of the surface since the sampling spots were selected in a random manner. It is also common to observe in bulk samples that the grinding of all components during the addition process is thought to result in their random separation. These EDX results show that the Y123 phase dominates in all prepared samples, which is in accord with XRD investigations.

Table 2. EDX analysis of chemical composition of Y123 with $x = (0.0, 0.2, 0.4, 0.6, 0.8, \text{ and } 1.0 \text{ wt.}\%) \text{ TiO}_2$.

TiO ₂ Addition wt.%	Atomic %					
	Y	Ba	Cu	O	Ti	Total
0.0	7.76	14.78	23.96	53.51	0.0	100%
0.2	7.39	12.66	25.16	54.80	0.0	100%
0.4	8.10	17.49	26.67	47.74	0.0	100%
0.6	6.43	14.24	22.30	49.20	7.82	100%
0.8	8.18	17.32	24.40	50.10	0.0	100%
1.0	3.12	37.51	12.45	30.68	16.25	100%

3.3. Alternating Current Susceptibility (ACS) Measurement

Figure 3 displays the AC susceptibility of real, χ' , and imaginary, χ'' , parts for the Y123 superconductor with different percentages of TiO₂ at $x = (0.0, 0.2, 0.4, 0.6, 0.8, \text{ and } 1.0 \text{ wt.}\%)$, measured at $H_{ac} = 5 \text{ Oe}$ and $f = 295 \text{ Hz}$. The values of the phase lock-in temperature, T_{cj} , and the diamagnetic onset temperature, $T_{c-onset}$, were determined from the plot of the peaks $d\chi'/dT$ versus T shown in Figure 4. It is noticed that for all added TiO₂ samples, the $T_{c-onset}$ showed a slight decrease with TiO₂ inclusion, while T_{cj} was greatly increased from 80.1 K for the pure Y123 samples to 91.5 K for 1.0 wt.% TiO₂. The increase in T_{cj} implies that the coupling between the grains was further enhanced with TiO₂. Based on the real part ($\chi'-T$), it is observed that the transition became sharper with TiO₂ addition compared to the non-added sample, which showed a two-step transition. This indicates a strong granular nature of these samples as the addition of TiO₂ nanoparticles increased. Furthermore, having a sharp transition in HTSC materials is evidence that the critical current density would be enhanced [33].

The Imaginary part, χ'' in the ($\chi''-T$) susceptibility displays the AC losses. Unlike the pure sample, two peaks were observed for TiO₂ samples, denoted as T_{pm} and T_{pg} , which correspond to inter-granular and intra-granular, respectively. The values of T_{pm} and T_{pg} are listed in Table 3. The loss peaks, T_{pg} , were found to occur at a higher temperature in samples with TiO₂ addition, revealing that dissipation for samples containing TiO₂ begins at higher temperatures. The sample with $x = 0.6$ exhibited the highest T_{pm} , whereas for other TiO₂ contents, T_{pm} slightly decreased as TiO₂ increased. This can be attributed to the inhibition of inter-grain coupling within the superconducting grains. It is known that the AC magnetic characteristics of high- T_c superconductors are caused by shielding currents that flow either inside the grains (intra-granular currents) or between grain boundaries (inter-granular currents) [34]. It should be noted that all Y123/TiO₂ composite samples showed weak peaks and broadening of the inter-granular peaks when compared to the pure sample. This indicated field penetration (due to granular quality) as well as hysteretic losses between grains [35]. The values of the inter-granular current density $J_c(T_{pm})$ for all samples were calculated using the Bean model equation $J_c(T_{pm}) = H/(ab)^{0.5}$ [36]. The value of $J_c(T_{pm})$ for all sintered samples was around 19 to 22 A/cm².

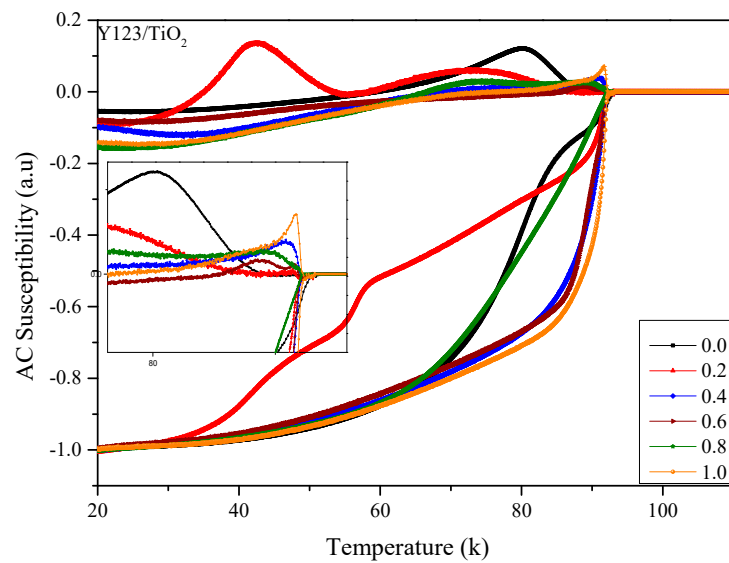


Figure 3. AC susceptibility ($\chi = \chi' + i\chi''$) versus temperature of Y123/(TiO₂)_x at $x = 0.0, 0.2, 0.4, 0.6, 0.8,$ and 1.0 wt.%, measured in a magnetic field of 5 Oe and at a frequency of 295 Hz.

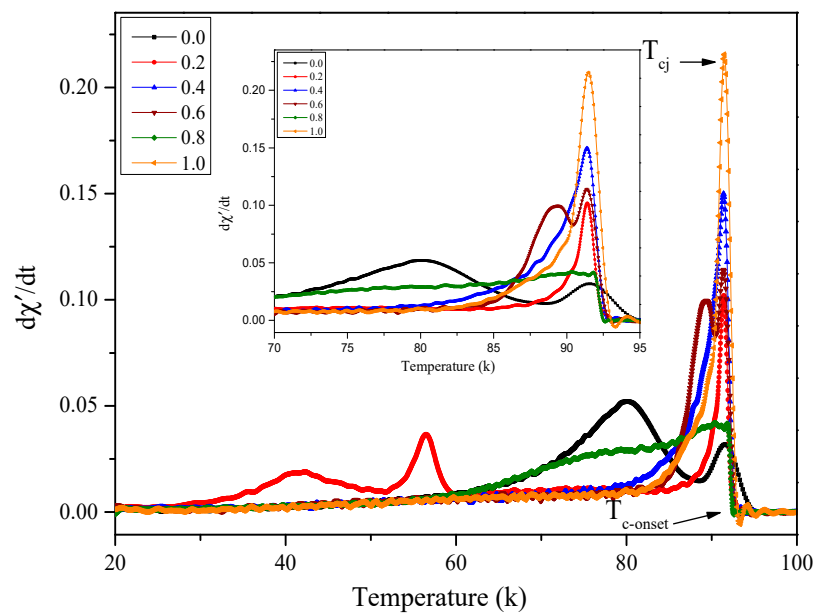


Figure 4. Derivative of the real part of AC susceptibility, $d\chi'/dT$, as a function of temperature of Y123/(TiO₂)_x at $x = 0.0, 0.2, 0.4, 0.6, 0.8,$ and 1.0 wt.%. The inset shows a magnified view of the region between 70 and 95 K.

Table 3. Summary data for $T_{c-onset}, T_{cj}, T_p, J_c(T_{pm}), I_0,$ and E_j of Y123/(TiO₂)_x at $x = 0.0, 0.2, 0.4, 0.6, 0.8,$ and 1.0 wt.%, measured in a magnetic field of 5 Oe and at a frequency of 295 Hz.

TiO ₂ Addition ($x = \text{wt.}\%$)	$T_{c-onset}$ (K)	T_{cj} (K)	T_p (K)		$J_c(T_{pm})$ (A/cm ²)	I_0 (μA)	$E_j \times 10^{-21}$ J
			T_{pg}	T_{pm}			
0.0	95.4	80.1	-	83.7	21.8	9.78	3.12
0.2	93.3	91.4	91.7	78.6	19.1	71.92	23.01
0.4	92.8	91.3	91.7	78.5	20.8	90.13	28.84
0.6	93	91.3	91.8	89	21.4	79.87	25.55
0.8	92.6	90.3	90.4	76	21.1	58.53	18.72
1.0	93.2	91.5	91.9	81.1	21.5	80.21	25.66

Due to the granular nature of ceramic superconductors, YBCO can be modelled as an array of weak Josephson junctions, with grain coupling occurring through Josephson currents. The maximum inter-grain Josephson current, I_0 , can be determined from the obtained values of T_{cj} and $T_{c-onset}$ using the following equations assumed by the Ambegaokar–Baratoff theory [37,38].

$$I_0 = 1.57 \times 10^{-8} \left(\frac{T_{c-onset}^2}{T_{c-onset} - T_{cj}} \right) \quad (1)$$

$$E_j = \frac{h}{4\pi e} I_0 \quad (2)$$

where h is Planck's constant, e is the electron's charge, and I_0 is the maximum Josephson current.

As revealed in Table 3, there was a remarkable increase in the values of I_0 and E_j for all samples with TiO_2 inclusion, with the highest value for the sample containing 0.4 wt.% TiO_2 addition. This result indicates that TiO_2 incorporation in YBCO bulk enhances the inter-grain coupling of the grains. Table 3 summarises the data for $T_{c-onset}$, T_p , T_{cj} , J_c (T_{pm}), I_0 , and E_j .

3.4. Electrical Resistivity Measurement

Normalised resistivity as a function of temperature is displayed in Figure 5a for $x = 0.0, 0.2, 0.4, 0.6, 0.8,$ and 1.0 wt.% TiO_2 added to Y123 bulk. The resistivity measurements were performed on bulk Y123 using the standard four-point probe technique in a temperature range of 30 to 280 K. All samples displayed a roughly linear drop in resistivity when cooled from room temperature to the critical onset temperature of the superconducting transition. Thus, a metal behaviour was confirmed for all Y123/ TiO_2 compounds. Analysing these curves showed a gradual degradation of the critical onset temperature, $T_{c-onset}$, up to 0.8 wt.% TiO_2 samples and then an increase for the sample at $x = 1.0$ wt.% TiO_2 . This decrease in $T_{c-onset}$, in comparison to pure Y123, could be due to secondary phase formation, the solidification process, or the effect of microscopic inhomogeneity in the Y123/ TiO_2 substance. The reduction in oxygen content in the CuO chains may be another satisfactory reason related to $T_{c-onset}$ degradation with TiO_2 addition [11,39]. The onset of superconducting transition temperature, $T_{c-onset}$, for a pure sample was observed at 95.6 K, which is consistent with the $T_{c-onset}$ value obtained by AC susceptibility (95.4 K). Notably, the decline in $T_{c-onset}$ measured by AC susceptibility and the four-point probe method has an almost similar trend, as shown in Figure 6, which displays the comparison results of $T_{c-onset}$ measured using the two methods. The electrical resistivity started to drop at 95.6, 93.1, 92.6, 92.5, 91.1, and 94.7 K, whereas it vanished at 91.7, 84.6, 89.1, 89, 87.2, and 91.7 K for $x = (0.0, 0.2, 0.4, 0.6, 0.8,$ and 1.0 wt.%) TiO_2 , respectively. The residual resistivity, ρ_0 , was decreased for all added samples, indicating improvement in weak links among the grains with TiO_2 nanoparticle inclusion. The sample at $x = 1.0$ wt.% was found to have the lowest value of ρ_0 . All determined values of the residual resistivity are presented in Table 4.

Table 4. Properties of superconducting transition temperature $T_{c-onset}$, $T_{c-offset}$, ΔT_c , residual resistivity, ρ_0 , and hole concentration, p , of Y123 at various wt.% TiO_2 addition.

TiO ₂ Addition	$T_{c-onset}$ (K)	$T_{c-offset}$ (K)	ΔT_c (K)	ρ_0 (Ω .cm)	Hole Concentration, p
0.0	95.6	91.7	3.9	0.61	0.160
0.2	93.1	84.6	8.5	0.45	0.142
0.4	92.6	89.1	3.5	0.41	0.140
0.6	92.5	89	3.5	0.44	0.140
0.8	91.2	87.2	4	0.37	0.138
1.0	94.7	91.7	3	0.30	0.149

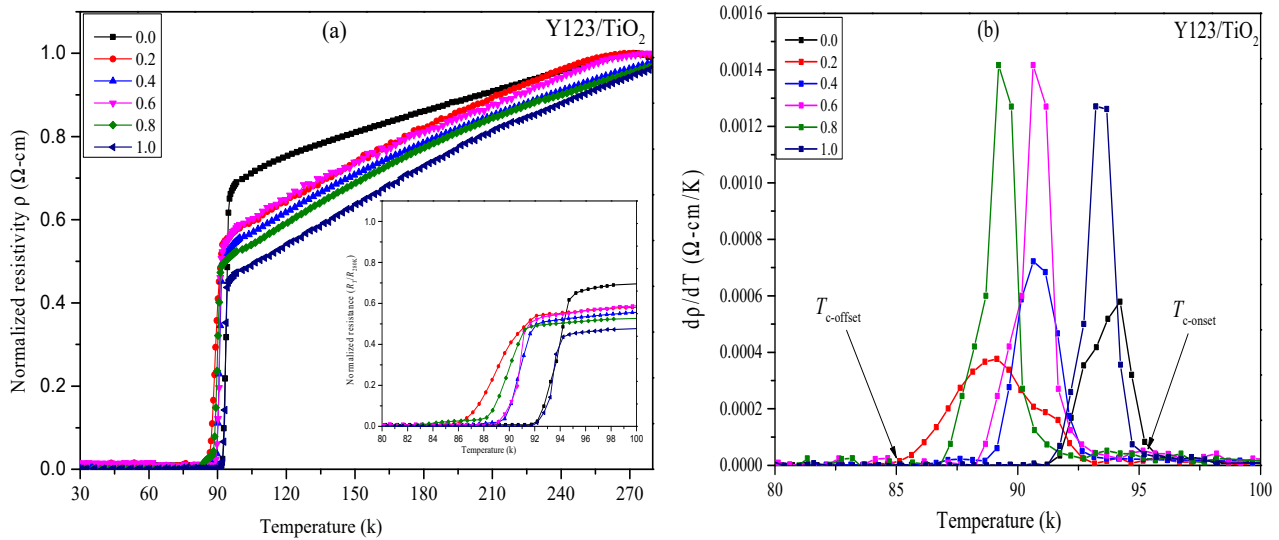


Figure 5. (a) Normalised resistivity versus temperature curve of Y123 samples with various wt.% of TiO₂; (b) derivative of resistivity against temperature of Y123 samples with various wt.% of TiO₂.

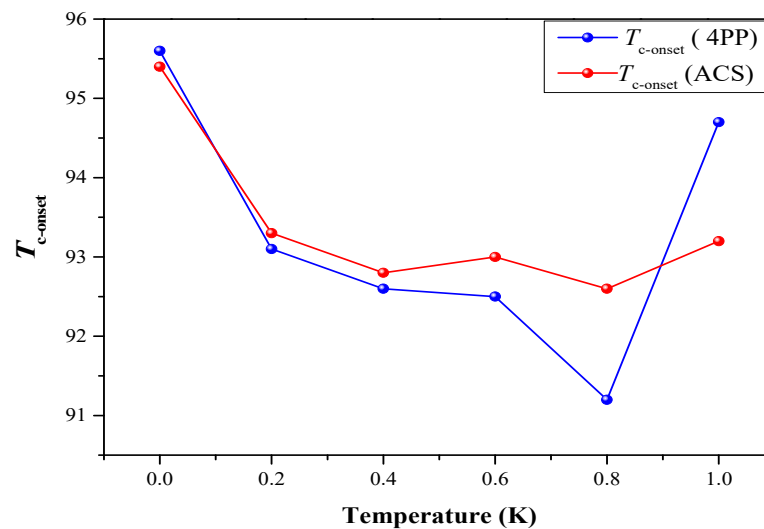


Figure 6. Comparison curves of $T_{c-onset}$ measured from 4PP and ACS for Y123 at $x = 0.0, 0.2, 0.4, 0.6, 0.8,$ and 1.0 wt.% TiO₂ addition.

More information about the transition can be obtained from the $d\rho/dT$ curves shown in Figure 5b. The transition width, ΔT_c , was around 3–4 K except at $x = 0.2$ wt.%, which exhibited a broadest ΔT_c of 8 K. Notably, the $d\rho/dT$ peaks of the high-level concentration of TiO₂ (0.6–1.0 wt.%) exhibited high and sharp peaks. It is believed that the improvement in the superconducting transition width is because of the modification effect of the TiO₂ inclusion on the grain boundary, which resulted in grain connectivity enhancement. Note that the sample with the highest concentration (1.0 wt.% TiO₂) showed the narrowest transition width, ΔT_c (3 K), and its peak was slightly shifted to a higher temperature. This result is consistent with the ACS result, as the same sample exhibited the sharpest and highest peak. These results suggest that a positive impact can be achieved as the concentration of TiO₂ increases. The hole concentration, p , in the CuO₂ plane was calculated using a well-known relation between T_c and the charge density [40].

$$p = 0.16 - \left[\left(1 - \frac{T_{c-onset}}{T_c^{max}} \right) / 82.6 \right]^{0.5} \quad (3)$$

where T_c^{max} in this study is 95.6 K for the YBCO phase, and p is the number of the hole concentration. The hole concentration decreased for all doped TiO₂ samples from 0.160 to 0.138. The change in oxygen content in the Y123 system may be responsible for this reduction in the charge carrier [41,42]. The summary of $T_{c-onset}$ (K), $T_{c-offset}$ (K), ΔT_c (K), and hole concentration, p , is listed in Table 4.

4. Conclusions

The composite ceramic Y123/(TiO₂) x ($x = 0.0, 0.2, 0.4, 0.6, 0.8,$ and 1.0 wt.%) synthesised by the thermal treatment method and annealed at 650 °C in a flowing oxygen atmosphere was successfully prepared. XRD analysis showed that an orthorhombic Y123 single-phase with a crystal structure was observed for all samples, with a trace to the Y211 secondary phase for the samples with TiO₂ addition. There was a slight dependence of the c -axis on TiO₂ concentration, which influenced the oxygen content ($7-\delta$). The orthorhombicity increased with TiO₂ addition, indicating better oxygen ordering. The findings of the FESEM analysis indicated that the incorporation of TiO₂ nanoparticles led to an increase in the average grain size, resulting in a reduction in pores and an overall increase in sample compactness. Electrical resistivity and AC susceptibility measurements showed that $T_{c-onset}$ was slightly decreased for all Y123/TiO₂ samples. The superconducting transition, ΔT_c , was improved with TiO₂ inclusion and was the sharpest at $x = 1.0$ wt.%. The residual resistivity, ρ_0 , decreased for all added samples, indicating a weak link improvement among the grains due to TiO₂ nanoparticle inclusion. From the AC susceptibility measurement, several significant parameters were determined and discussed. The results showed a significant increase in the values of I_0 and E_j for all samples with TiO₂. This suggests that the addition of TiO₂ enhanced the inter-grain coupling by improving grain connectivity as it incorporated between the grains and served as efficient pinning centres inside the Y123 ceramic. These results prove the positive impact of TiO₂ on Y123 performance.

Author Contributions: Conceptualization, F.B., M.M.A.K. and M.M.; methodology, F.B. and K.K.M.S.; software, F.B., N.E.S. and A.H.; validation, F.B., C.S.K. and L.K.P.; formal analysis, F.B., T.S.T. and A.H.S.; investigation, F.B., M.M.A.K. and M.M.; resources, F.B. and M.M.A.K.; data curation, F.B., K.J.H., M.K.A.K. and M.K.S.; writing—original draft preparation, F.B.; writing—review and editing, M.M.A.K., M.M. and H.B.; project administration, M.M.A.K. and M.M.; funding acquisition, M.M.A.K. and M.M. All authors have read and agreed to the published version of the manuscript.

Funding: This research was funded by the Ministry of Higher Education (MOHE) Malaysia under FRGS Grant No. FRGS/1/2017/STG02/UPM/02/4 and Universiti Putra Malaysia IPS Grant No. 9666600.

Institutional Review Board Statement: Not applicable.

Informed Consent Statement: Not applicable.

Data Availability Statement: The data presented in this study are available on request from the corresponding author. The data are not publicly available due to ethical restrictions.

Acknowledgments: Additionally, this work was partly supported partly supported by Japan Science and Technology (JST) for the Advanced Project Based Learning (aPBL), Shibaura Institute of Technology. The authors would like to thank the valuable support and discussions by all members of the Superconductor and Thin Films Laboratory of Universiti Putra Malaysia.

Conflicts of Interest: The authors declare no conflict of interest.

References

1. Chu, C.W. Superconductivity above 90 K. *Proc. Natl. Acad. Sci. USA* **1987**, *84*, 4681–4682. [[CrossRef](#)]
2. Hassenzahl, W.V. Superconductivity, an enabling technology for 21st century power systems? *IEEE Trans. Appl. Supercond.* **2001**, *11*, 1447–1453. [[CrossRef](#)]
3. Kelley, N.; Nassi, M.; Masur, L. Application of HTS wire and cables to power transmission: State of the art and opportunities. In Proceedings of the IEEE Power Engineering Society Transmission and Distribution Conference, Columbus, OH, USA, 28 January 2001–1 February 2001; Volume 2, pp. 448–454. [[CrossRef](#)]

4. Bishop, D.J.; Gammel, P.L.; Huse, D.A.; Murray, C.A. Magnetic Flux-Line Lattices and Vortices in the Copper Oxide Superconductors. *Science* **1992**, *255*, 165–172. [[CrossRef](#)]
5. Larbalestier, D. Superconductor Flux Pinning and Grain Boundary Control. *Science* **1996**, *274*, 736–737. [[CrossRef](#)]
6. Haugan, T.; Barnes, P.N.; Wheeler, R.; Meisenkothen, F.; Sumption, M. Addition of nanoparticle dispersions to enhance flux pinning of the $\text{YBa}_2\text{Cu}_3\text{O}_{7-x}$ superconductor. *Nature* **2004**, *430*, 867–870. [[CrossRef](#)]
7. Çakır, B.; Aydiner, A.; Basoglu, M.; Yanmaz, E.; Aydiner, A. The Effect of Y_2O_3 on AC Susceptibility Measurements of MPMG YBCO Superconductor. *J. Supercond. Nov. Magn.* **2013**, *26*, 937–941. [[CrossRef](#)]
8. Almessiere, M.A.; Slimani, Y.; Hannachi, E.; Algarni, R.; Ben Azzouz, F. Impact of Dy_2O_3 nanoparticles additions on the properties of porous YBCO ceramics. *J. Mater. Sci. Mater. Electron.* **2019**, *30*, 17572–17582. [[CrossRef](#)]
9. Slimani, Y.; Almessiere, M.; Hannachi, E.; Mumtaz, M.; Manikandan, A.; Baykal, A.; Ben Azzouz, F. Improvement of flux pinning ability by tungsten oxide nanoparticles added in $\text{YBa}_2\text{Cu}_3\text{O}_y$ superconductor. *Ceram. Int.* **2019**, *45*, 6828–6835. [[CrossRef](#)]
10. Dadras, S.; Falahati, S.; Dehghani, S. Effects of graphene oxide doping on the structural and superconducting properties of $\text{YBa}_2\text{Cu}_3\text{O}_{7-\delta}$. *Phys. C Supercond. Its Appl.* **2018**, *548*, 65–67. [[CrossRef](#)]
11. Mellekh, A.; Zouaoui, M.; Ben Azzouz, F.; Annabi, M.; Ben Salem, M. Nano- Al_2O_3 particle addition effects on Y $\text{Ba}_2\text{Cu}_3\text{O}_y$ superconducting properties. *Solid State Commun.* **2006**, *140*, 318–323. [[CrossRef](#)]
12. Zhang, Y.; Zhou, S.; Wang, X.; Dou, S.X. Effect of addition of nanoparticle $\text{TiO}_2/\text{SiO}_2$ on the superconducting properties of MgB_2 . *Phys. C Supercond. Its Appl.* **2008**, *468*, 1383–1386. [[CrossRef](#)]
13. Prokhorov, V.G.; Svetchnikov, V.L.; Park, J.S.; Kim, G.H.; Lee, Y.P.; Kang, J.-H.; Khokhlov, V.A.; Mikheenko, P. Flux pinning and the paramagnetic Meissner effect in MgB_2 with TiO_2 inclusions. *Supercond. Sci. Technol.* **2009**, *22*, 045027. [[CrossRef](#)]
14. Kishan, H.; Awana, V.; de Oliveira, T.; Alam, S.; Saito, M.; de Lima, O. Superconductivity of nano- TiO_2 -added MgB_2 . *Phys. C Supercond. Its Appl.* **2007**, *458*, 1–5. [[CrossRef](#)]
15. Pham, A.T.; Tran, D.T.; Vu, L.H.; Chu, N.T.; Thien, N.D.; Nam, N.H.; Binh, N.T.; Tai, L.T.; Hong, N.T.; Long, N.T.; et al. Effects of TiO_2 nanoparticle addition on the flux pinning properties of the $\text{Bi}_{1.6}\text{Pb}_{0.4}\text{Sr}_2\text{Ca}_2\text{Cu}_3\text{O}_{10+\delta}$ ceramics. *Ceram. Int.* **2022**, *48*, 20996–21004. [[CrossRef](#)]
16. Hamid, N.A.; Abd-Shukor, R. Effects of TiO_2 addition on the superconducting properties of Bi-Sr-Ca-Cu-O system. *J. Mater. Sci.* **2000**, *35*, 2325–2329. [[CrossRef](#)]
17. Ghahramani, S.; Shams, G.; Soltani, Z. Comparative Investigation of the Effect of Titanium Oxide Nanoparticles on Some Superconducting Parameters of $\text{Y}_3\text{Ba}_5\text{Cu}_8\text{O}_{18\pm\delta}$ and $\text{Y}_1\text{Ba}_2\text{Cu}_3\text{O}_{7-\delta}$ Composites. *J. Electron. Mater.* **2021**, *50*, 4727–4740. [[CrossRef](#)]
18. Rejith, P.; Vidya, S.; Thomas, J. Improvement of Critical Current Density in $\text{YBa}_2\text{Cu}_3\text{O}_{7-\delta}$ Superconductor with Nano TiO_2 Addition. *Mater. Today Proc.* **2015**, *2*, 997–1001. [[CrossRef](#)]
19. Hannachi, E.; Slimani, Y.; Ben Azzouz, F.; Ekicibil, A. Higher intra-granular and inter-granular performances of YBCO superconductor with TiO_2 nano-sized particles addition. *Ceram. Int.* **2018**, *44*, 18836–18843. [[CrossRef](#)]
20. Kebbede, A.; Parai, J.; Carim, A.H. Sol-gel coating of $\text{YBa}_2\text{Cu}_3\text{O}_{7-x}$ with TiO_2 for enhanced anisotropic grain growth. *Energy* **1993**, *51*, 2845–2851.
21. Yusuf, N.N.M.; Kechik, M.M.A.; Baqiah, H.; Kien, C.S.; Pah, L.K.; Shaari, A.H.; Jusoh, W.N.W.W.; Sukor, S.I.A.; Dihom, M.M.; Talib, Z.A.; et al. Structural and Superconducting Properties of Thermal Treatment-Synthesised Bulk $\text{YBa}_2\text{Cu}_3\text{O}_{7-\delta}$ Superconductor: Effect of Addition of SnO_2 Nanoparticles. *Materials* **2019**, *12*, 92. [[CrossRef](#)]
22. Dihom, M.M.; Shaari, A.H.; Baqiah, H.; Al-Hada, N.M.; Kien, C.S.; Azis, R.S.; Kechik, M.M.A.; Talib, Z.A.; Abd-Shukor, R. Microstructure and superconducting properties of Ca substituted $\text{Y}(\text{Ba}_1-\text{Ca})_2\text{Cu}_3\text{O}_{7-\delta}$ ceramics prepared by thermal treatment method. *Results Phys.* **2017**, *7*, 407–412. [[CrossRef](#)]
23. Dihom, M.M.; Shaari, A.H.; Baqiah, H.; Al-Hada, N.M.; Talib, Z.A.; Kien, C.S.; Azis, R.S.; Kechik, M.M.A.; Pah, L.K.; Abd-Shukor, R. Structural and superconducting properties of $\text{Y}(\text{Ba}_1-\text{K})_2\text{Cu}_3\text{O}_{7-\delta}$ ceramics. *Ceram. Int.* **2017**, *43*, 11339–11344. [[CrossRef](#)]
24. Kamarudin, A.N.; Kechik, M.M.A.; Abdullah, S.N.; Baqiah, H.; Chen, S.K.; Karim, M.K.A.; Ramli, A.; Lim, K.P.; Shaari, A.H.; Miryala, M.; et al. Effect of Graphene Nanoparticles Addition on Superconductivity of $\text{YBa}_2\text{Cu}_3\text{O}_{7-\delta}$ Synthesized via the Thermal Treatment Method. *Coatings* **2022**, *12*, 91. [[CrossRef](#)]
25. Dihom, M.M.; Shaari, A.H.; Baqiah, H.; Al-Hada, N.M.; Chen, S.K.; Azis, R.S.; Kechik, M.M.A.; Abd-Shukor, R. Effects of Calcination Temperature on Microstructure and Superconducting Properties of Y123 Ceramic Prepared Using Thermal Treatment Method. *Solid State Phenom.* **2017**, *268*, 325–329. [[CrossRef](#)]
26. Slimani, Y.; Hannachi, E.; Ekicibil, A.; Almessiere, M.; Ben Azzouz, F. Investigation of the impact of nano-sized wires and particles TiO_2 on Y-123 superconductor performance. *J. Alloys Compd.* **2019**, *781*, 664–673. [[CrossRef](#)]
27. Chamekh, S.; Bouabellou, A. The Effects of Magnetic Dopant on the Structural and Electrical Properties in Superconducting $\text{YBaCu}_3\text{O}_{7-\delta}$ Ceramic. *Adv. Chem. Eng. Sci.* **2018**, *8*, 1–10. [[CrossRef](#)]
28. Cava, R.J.; Batlogg, B.; Chen, C.H.; Rietman, E.A.; Zahurak, S.M. Oxygen stoichiometry, superconductivity and normal-state properties of $\text{YBa}_2\text{Cu}_3\text{O}_{7-o}$. *Nature* **1987**, *329*, 9–11. [[CrossRef](#)]
29. Benzi, P.; Bottizzo, E.; Rizzi, N. Oxygen determination from cell dimensions in YBCO superconductors. *J. Cryst. Growth* **2004**, *269*, 625–629. [[CrossRef](#)]
30. Maaz, K.; Karim, S.; Mumtaz, A.; Hasanain, S.; Liu, J.; Duan, J. Synthesis and magnetic characterization of nickel ferrite nanoparticles prepared by co-precipitation route. *J. Magn. Magn. Mater.* **2009**, *321*, 1838–1842. [[CrossRef](#)]

31. Hsiao, Y.-J.; Chang, Y.-H.; Chang, Y.-S.; Fang, T.-H.; Chai, Y.-L.; Chen, G.-J.; Huang, T.-W. Growth and characterization of NaNbO₃ synthesized using reaction-sintering method. *Mater. Sci. Eng. B Solid. State Mater. Adv. Technol.* **2007**, *136*, 129–133. [[CrossRef](#)]
32. Awano, M.; Fujishiro, Y.; Moon, J.; Takagi, H.; Rybchenko, S.; Bredikhin, S. Microstructure control of an oxide superconductor on interaction of pinning centers and growing crystal surface. *Phys. C Supercond. Its Appl.* **2000**, *341–348*, 2017–2018. [[CrossRef](#)]
33. Uysal, E.; Ozturk, A.; Kutuk, S.; Çelebi, S. Effects of Lu Doping on the Magnetic Behavior of YBCO Superconductors Prepared by MPMG Method. *J. Supercond. Nov. Magn.* **2014**, *27*, 1997–2003. [[CrossRef](#)]
34. Vanderbemden, P.; Cloots, R.; Ausloos, M.; Doyle, R.; Bradley, A.; Lo, W.; Cardwell, D.; Campbell, A. Intragranular and intergranular superconducting properties of bulk melt-textured YBCO. *IEEE Trans. Appl. Supercond.* **1999**, *9*, 2308–2311. [[CrossRef](#)]
35. Arlina, A.; Halim, S.; Kechik, M.A.; Chen, S. Superconductivity in Bi–Pb–Sr–Ca–Cu–O ceramics with YBCO as additive. *J. Alloys Compd.* **2015**, *645*, 269–273. [[CrossRef](#)]
36. Bean, C.P. Magnetization of High-Field Superconductors. *Rev. Mod. Phys.* **1964**, *267*, 31–39. [[CrossRef](#)]
37. Clem, J.R. Granular and superconducting-glass properties of the high-temperature superconductors. *Phys. C Supercond. Its Appl.* **1988**, *153–155*, 50–55. [[CrossRef](#)]
38. Ambegaokar, V.; Baratoff, A. Tunneling Between Superconductors. *Phys. Rev. Lett.* **1963**, *11*, 104. [[CrossRef](#)]
39. Brecht, E.; Schmahl, W.; Mieke, G.; Rodewald, M.; Fuess, H.; Andersen, N.; Hanßmann, J.; Wolf, T. Thermal treatment of YBa₂Cu_{3–x}Al_xO_{6+δ} single crystals in different atmospheres and neutron-diffraction study of excess oxygen pinned by the Al substituents. *Phys. C Supercond. Its Appl.* **1996**, *265*, 53–66. [[CrossRef](#)]
40. Presland, M.; Tallon, J.; Buckley, R.; Liu, R.; Flower, N. General trends in oxygen stoichiometry effects on T_c in Bi and Tl superconductors. *Phys. C Supercond. Its Appl.* **1991**, *176*, 95–105. [[CrossRef](#)]
41. Bernhard, C.; Shaked, H. Generic superconducting phase behavior in high- T_c cuprates: T_c variation with hole concentration in YBa₂Cu₃O_{7–δ}. *Phys. Rev. B* **1995**, *51*, 911–914.
42. Panagopoulos, C.; Xiang, T. Relationship between the Superconducting Energy Gap and the Critical Temperature in High-T_c Superconductors. *Phys. Rev. Lett.* **1998**, *81*, 2336–2339. [[CrossRef](#)]

Disclaimer/Publisher’s Note: The statements, opinions and data contained in all publications are solely those of the individual author(s) and contributor(s) and not of MDPI and/or the editor(s). MDPI and/or the editor(s) disclaim responsibility for any injury to people or property resulting from any ideas, methods, instructions or products referred to in the content.